ANNUAL REVIEWS

Annual Review of Condensed Matter Physics

Topographic Mechanics and Applications of Liquid Crystalline Solids

Mark Warner

Cavendish Laboratory, University of Cambridge, Cambridge CB3 0HE, United Kingdom; email: mw141@cam.ac.uk

Annu. Rev. Condens. Matter Phys. 2020. 11:125–45

First published as a Review in Advance on October 21, 2019

The *Annual Review of Condensed Matter Physics* is online at conmatphys.annualreviews.org

https://doi.org/10.1146/annurev-conmatphys-031119-050738

Keywords

curvature, responsive, actuation, photo

Abstract

Liquid crystal elastomers and glasses suffer huge length changes on heating, illumination, exposure to humidity, etc. A challenge is to program these changes to give a complex mechanical response for micromachines and soft robotics. Also desirable can be strong response, where bend is avoided in favor of stretch and compression, even in the slender shells that are our subject.

A new mechanics paradigm arises from such materials—spatially programmed anisotropy allows a spatially varying metric to develop upon stimulation, with evolving Gaussian curvature, topography changes, and superstrong actuation. We call this metric mechanics or topographical mechanics. Thus programmed, liquid crystalline solids meet the above aims.

A frontier is the complete programming and control of topography, driving both Gaussian and mean curvature evolution. That, and smart shells, which sense and self-regulate, and exotic new realizations of anisotropic responsive structures, are our concluding themes.

1. CURVATURE CHANGE AND MECHANICS

We review the formation of shells with intrinsic curvature from flat sheets resulting from heating, illumination, and differential swelling. This control of topography leads to new paradigms for exploiting the elasticity of mechanically responsive solids. We have termed this topographic mechanics in our title, but might equally have called it metric mechanics because it is the control over changing lengths in the plane that leads to Gaussian curvature (GC) evolving without elastic stress. Conversely, blocking this curved topography development leads to very large (stretch) stresses, with possible new applications in actuation and microcontrol. Our materials are liquid crystalline (LC) solids—elastomers and glasses. We ask, how are they driven and what are their material commonalities and differences? Heat, light, solvent, and pH are all effective in giving reversible strains between 10% and 400%, with moduli in the range of 10^9–10^5 Pa, for glasses and elastomers, respectively.

Contraction along an LC ordering direction, i.e., the director **n**, can generate a pull in a strip with **n** along its length if the contraction is blocked (e.g., by clamping). But if the body is slender, e.g., when there is elongation during recovery, then push is impossible due to Euler bend instabilities. Bend is a much lower energy alternative to compression during push. We find that mechanics more complex than pull without push is achievable from complex directors leading to several possible types of topography change. The idea is encapsulated by the observation of Bhattacharya & James: At the small scale, "The material is the machine" (1), without gears, cogs, or pistons (see **Figure 1**). Thus, our recurrent theme is the control of intrinsic curvature, incurring stretch or compression in materials if they are loaded and the load frustrates curvature change. This paradigm contrasts with the introduction of bend—extrinsic curvature in one direction—which is much weaker.[1]

This review first discusses the materials necessary for the complex mechanics that are then sketched. We conclude by looking at future and wider perspectives to achieve the complete control of curvature and shape, and at other developments involving quite different materials and length scales as well as control, autonomy, and adaptability of shells for use in robotics.

Two leading figures in the field, Broer and White, have comprehensively reviewed the chemistry, the physical phenomena, the creation of shells, and the translation to mechanics (2) in the aptly titled paper "Programmable and Adaptive Mechanics with Liquid Crystal Polymer Networks and Elastomers," to which the reader is referred.

2. METRIC-CHANGING MATERIALS

Nematic LC solids are the most studied, but there are also cholesteric and smectic elastomers and glasses, all with fascinating properties. The generality of LC elastomers is discussed in a book (3), including exploring LC ordering, elasticity, networks, LC solid elasticity, and more complex phases. The book's first chapter is available free online and offers a bird's-eye view (4) of these materials. We only consider nematics here because they alone have been used for this kind of topography change. Nematic glasses are much less well understood, with the exception of aspects of their photoresponse.

2.1. LC Solids

Essential to nematics are molecular rods that orientationally order about a director **n** on cooling. **Figure 2*a*** shows a computer realization of a disordered system of molecular rods being cooled

[1] Bend can be very desirable if (*a*) long strokes are needed and (*b*) the forces required are comparable with those delivered by blocked bend. It is a question of mechanical impedance between the deformation route and the task.

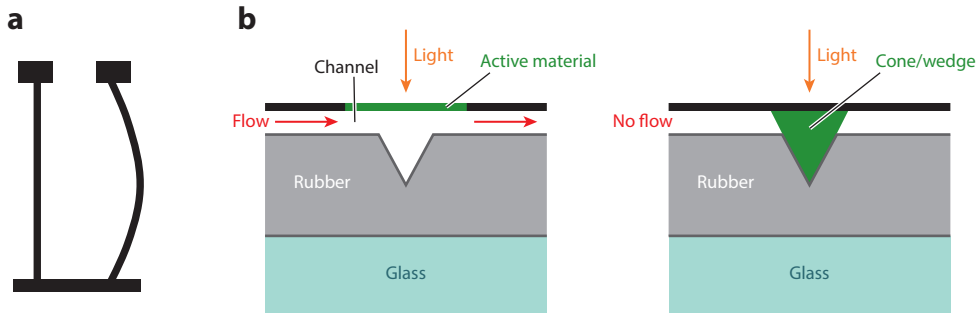

Figure 1

(*a*) A slender rod or slender sheet seen in section. On elongating its natural length, it fails to push up a load, but rather buckles to accommodate its extra length without compression. (*b*) An active region of flat sheet transforming to a strong topography on illumination and blocking a channel off—an example of the machine's function being encoded into the material (see Reference 1).

to an ordered, nematic phase with its director indicated. Rods can be connected together by flexible spacers to form linear polymers, with rods in the backbone or pendant to it. Either way, rod ordering produces anisotropy in the shape distribution of the polymers. If these chains are cross-linked together to form a solid, it too suffers mechanical shape changes, mirroring molecular response. These spontaneous responses to order change are distortions of ~20–400% for LC elastomers, and 3–15% for LC glasses. A typical molecular rod is shown below the phases with its stiff core and flexible spacers allowing it to be concatenated N times to form a polymer liquid crystal. **Figure 2*b*** is a cartoon of a block of nematic rubber formed by linking the chains together. The connectivity, and hence mechanics, is via the backbones (shown), and the rods that create the order are suppressed for clarity in the diagram, but see the inset. The extension by a factor λ along **n**, and the perpendicular contractions $1/\sqrt{\lambda}$, are shown in the cooled (*right*) block relative to the

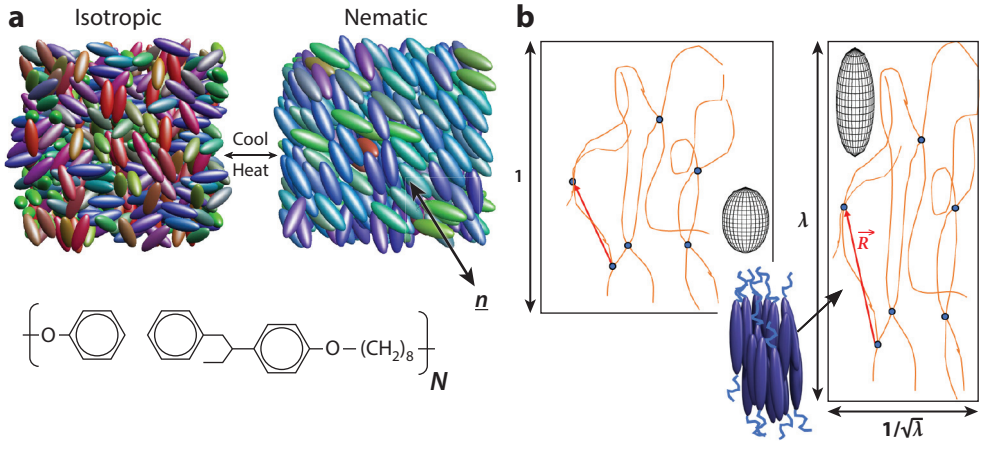

Figure 2

(*a*) Computer realizations of isotropic and nematic phases of rods, and a typical rod molecule of such phases, but additionally with spacers/connectors that allow it to be concatenated to be a polymer. (*b*) Blocks of rubber composed of chains cross-linked together. A less anisotropic system (*left*) is further cooled to higher anisotropy and thereby elongates by a factor λ. Panel *a* provided by D.J. Cleaver.

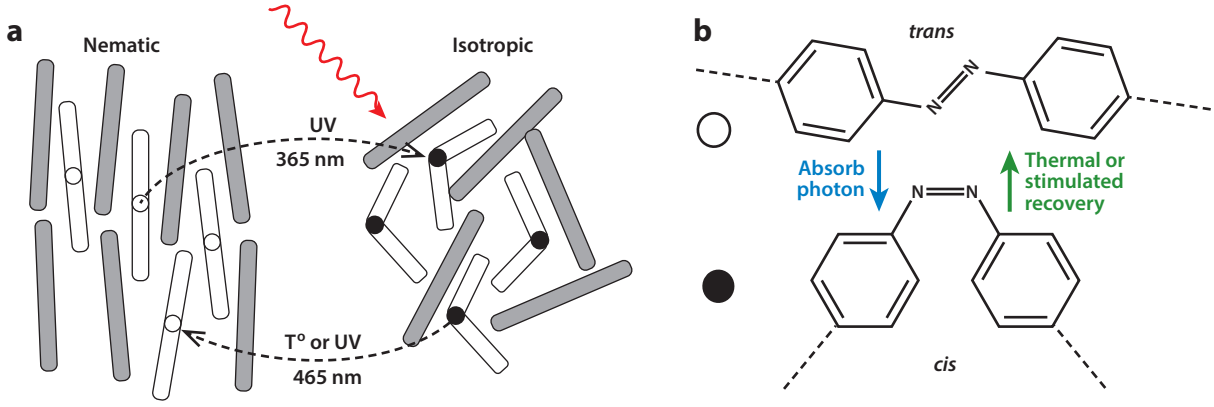

Figure 3

(*a*) Conventional (*gray*) host and guest photorods with a dye core (*circle*) that can absorb a photon and bend, thereby lowering nematic order of the fluid. (*b*) The straight (ground-state *trans*) and bend (excited state *cis*) forms of the dye core of the guest photorods. Here, the dye is azobenzene.

dimension 1 in the higher temperature block (*left*). Spheroids of varying anisotropy represent the second moment of the molecular shape distributions.

Their low moduli (10^5–10^6 Pa) and huge distortions are because elastomers are only marginally solid. Indeed, at the molecular scale they have the mobility of liquids. Thus, classically, or as liquid crystalline elastomers (LCEs), with deformations imposed or spontaneous, rubbers respond at constant volume; hence, the $1/\sqrt{\lambda}$ factor changes perpendicular to **n**. The directors of LCEs can be induced to rotate by mechanical fields, and a deeply subtle and interesting elasticity ensues. We ignore that here and concentrate only on shape change resulting from changes in the magnitude, rather than direction, of nematic order. Because tension will be mostly along the director, or the order has vanished with temperature or illumination, then director rotation will not be an issue.

Glasses are more tightly cross-linked, mobility is limited, and moduli are high ($\gtrsim 10^9$ Pa); thus, distortions are smaller. Nematic elastomers are well understood using statistical mechanics applied to molecular shape distributions as for classical elastomers. However, such a depth of understanding and modeling of shape changes and elasticity of LC glasses is lacking. It is known that free volume increases, but from distortions unequal along and perpendicular to **n**, as temperature rises. Such directional thermal response has been exploited by imprinting complex director variation through the thickness of glassy LC cantilevers. For instance, greater contraction around one surface in which the director is along the cantilever, and expansion along the cantilever near the other surface, where the director is perpendicular, leads to bend (5). Although we do not pursue bend, such director patterning lays the groundwork for our topography-changing shells. Another, important, typography that we do not pursue is that of anchored layers that change their surfaces in response to localized volume changes, induced thermally in patterns or by photoresponse as below (6).

2.2. Photomechanics of LC Solids

An optically driven reduction of nematic order, and hence an optomechanical response, is possible when there are guest photorods with a photoisomerizing dye species at their core. Absorbing a photon turns the dye from its straight *trans* to its bent *cis* state (see **Figure 3*a***). The rod sections pendant to the central core are no longer collinear and the large, now bent guest photorods reduce the order of their conventional rod hosts. If the rods are part of a polymer liquid crystal network,

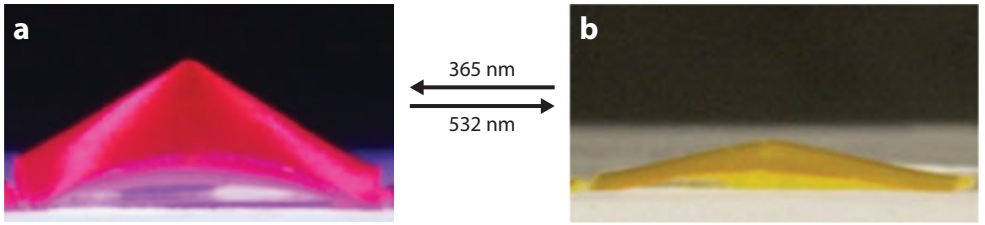

Figure 4

Photoswitching between (*a*) a photoexcited state (with its mechanical response) and (*b*) the ground state (which has recovered from its mechanical distortion). Photos provided by Tim White; see Reference 15 for more examples.

there is then a contraction along the director [see References 7–10 for LC photoelastomers and Yu et al. (11) and Harris et al. (12) for early work on LC photoglasses]. A book edited by White (13) comprehensively reviews photomechanical materials and their exploitation. See also the review by White & Boer (2). For many elastomers, one can directly map their photoresponse onto their simple thermal response because there is a common cause—the reduction in order (7). The magnitude of photomechanics in LC solids (10–400%) is unparalleled in other systems. Other advantages are that light can be delivered remotely (unlike electricity) very quickly and can be pulsed, and its color can be varied.

Directionality is intrinsic to the response and leads to rich possibilities, for instance, the control of mechanics also by light polarization: If the light's electric vector **E** is along **n**, it is generally more likely to be absorbed because the dye's absorption dipole is typically along the rod, itself aligned with **n**. Thus contraction is greater where **E** and **n** are parallel. A beautiful example of picking out directions is that of polarized light striking a polydomain LC solid, where domains along **E** evidently contract more than others, and thereby give a polarization-dependent macroscopic contraction along **E**, a response that changes when **E** is rotated [see Yu et al. (11) for glasses and Harvey & Terentjev (14) for elastomers].

Dyes differ greatly in their response to light and their modes of recovery after illumination. Most dyes recover their ground state by thermal back reactions and light-induced back reactions (stimulated decay of the *cis* state). The time of thermal decay can range hugely from milliseconds to days. Optical recovery depends on the wavelength of light (always longer than the primary beam's wavelength) and on its intensity. An excellent investigation of both recovery routes is from White and colleagues (15), where recovery of mechanical distortion induced by 365-nm light can be achieved in a few minutes by light of 532 nm, rather than over hours if by thermal recovery (see **Figure 4**).

Some dyes can recover only by optical stimulation. These present an advantage in that, once a deformed state has been induced, no further optical power is required to maintain it. Later switching to another configuration can be done at will.

If the return rate, for instance thermal, is slow compared with the forward rate (determined by the incident intensity), the *trans* population becomes depleted. The absorption is reduced and light can penetrate more deeply to then deplete *trans* species still further into the solid. The Beer law attenuation of intensity with depth, $I(z) = I_0 e^{-z/d}$, no longer holds (16). (d is the Beer penetration depth, dependent on dye concentration and wavelength, z the depth, and I_0 the incident intensity.) Instead $I(z)$ diminishes linearly until too weak to significantly deplete the *trans* population, and Beer's law is reasserted. The deviation from Beer is in practice extremely important. The length d is typically much less than the thickness of photosheets and beams. For appreciable mechanical response to take place, an appreciable fraction of the sample volume must be illuminated, and that

can only take place if penetration is deeper than d. The *trans* population can be explicitly measured by a weaker beam that does not cause significant population change itself. In this context, *trans* population depletion and its recovery have been measured at the same time as the mechanical distortion (15). This careful investigation connects photostimulation and mechanical response, given that hours can elapse and temperature has equilibrated. Diminishing intensity with depth because of absorption means diminishing contractions and, thus, cantilevers can bend, usually toward the incident light [see Camacho-Lopez et al. (10) for a very early example of a photodriven beam, achieving 45° bend in 60 ms]. As yet another example of polarization dependence, White et al. (17–19) showed a cantilever in which bend, relative to the incidence side of the illuminating light, reverses according to whether the light is polarized parallel or perpendicular to the cantilever's axis.

Other authors have instead found the mechanical response to be photothermal; that is, heat generated by light absorption is responsible for the mechanical distortions they observe (20–22). It is also clear there are dynamical effects associated with the process of isomerization and the creation of free volume. Liu & Broer (6) found that irradiating simultaneously with the color for forward reaction and with that for recovery greatly increased the free volume production. Furthermore, the recovery of free volume after ceasing to irradiate was very rapid compared with the decay of the *cis* population to *trans*, suggesting that the geometric shape of the bent rods was not the only impetus in glassy systems for mechanical distortion. See also a discussion, along with details of free volume changes, in Reference 23 and analogously differences in cone recovery and isomerization in Reference 15. We now show how such materials' responses can be harnessed to great effect by taking a director geometry more subtle than linear or polydomain.

3. CURVATURE AND THE INDUCTION OF TOPOGRAPHY CHANGE

To modify the topography, and above all the GC, of sheets, we need to control distances between material points in the surface. At our disposal in LC solids are contraction/elongation factors, $\lambda < 1$ and $\lambda > 1$, respectively, along the director, with corresponding factors $\lambda^{-\nu} > 1$ and $\lambda^{-\nu} < 1$ perpendicular to the director accompanying the respective contractions/elongations. The exponent ν corresponds to a Poisson ratio in small extension elasticity in which an imposed contraction along one direction leads to perpendicular elongations, and vice versa for imposed elongations. However, here the effect is due to spontaneous length changes along $\mathbf{n}$, and we call ν an optothermal Poisson ratio. Elastomers have $\nu = \frac{1}{2}$, and glasses have $\nu \in (1/2, 2)$ roughly. Volume changes on distortion, $V \to V'$, considering changes in lineal dimensions by the λ factors along the edges of a small cube aligned locally with $\mathbf{n}$, are

$$V'/V = \lambda \times \lambda^{-\nu} \times \lambda^{-\nu} = \lambda^{1-2\nu}. \qquad 1.$$

Rubber is volume conserving, $\nu = \frac{1}{2}$, whereas glass has $\nu > \frac{1}{2}$, with volume increase upon contraction along $\mathbf{n}$.

The stretches and contractions associated with the thermal and photo-distortions discussed above are elements of the deformation gradient tensor, $\underline{\underline{\boldsymbol{\lambda}}} = \partial \boldsymbol{R}/\partial \boldsymbol{R}_0$, where $\boldsymbol{R}_0$ is a material point in the reference state (our initial, flat sheet) that maps to $\boldsymbol{R}$ in the target state. It corresponds to the local stretches we have defined and can be compactly written:

$$\underline{\underline{\boldsymbol{\lambda}}} = \left(\lambda - \lambda^{-\nu}\right) \mathbf{nn} + \lambda^{-\nu} \underline{\underline{\boldsymbol{\delta}}} \equiv \begin{pmatrix} \lambda^{-\nu} & 0 & 0 \\ 0 & \lambda^{-\nu} & 0 \\ 0 & 0 & \lambda \end{pmatrix}. \qquad 2.$$

The latter is in Cartesian coordinates based on $\mathbf{n}$ along $\mathbf{z}$. Check that the former gives in the latter the right entries along and perpendicular to $\mathbf{n}$. Check also that $V'/V = \mathrm{Det}(\underline{\underline{\boldsymbol{\lambda}}})$—the product of

the diagonal values. The fractional volume change is an invariant of the $\underline{\underline{\lambda}}$ tensor; it does not matter which frame we find volume changes in.

These ideas are the machinery for describing length changes and curvature: The change in the (squared) change in length ds of an element $d\mathbf{R}_0$ in becoming $d\mathbf{R}$, that is $d\mathbf{R} \equiv \underline{\underline{\lambda}} \cdot d\mathbf{R}_0$, emerges from

$$(d\mathbf{R})^2 = (\underline{\underline{\lambda}} \cdot d\mathbf{R}_0)^{\mathrm{T}} \cdot (\underline{\underline{\lambda}} \cdot d\mathbf{R}_0) = d\mathbf{R}_0^{\mathrm{T}} \cdot (\underline{\underline{\lambda}}^{\mathrm{T}} \cdot \underline{\underline{\lambda}}) d\mathbf{R}_0,$$

$$(ds)^2 = (d\mathbf{R})^2 - (d\mathbf{R}_0)^2 = d\mathbf{R}_0^{\mathrm{T}} \cdot (\underline{\underline{g}} - \underline{\underline{\delta}}) \cdot d\mathbf{R}_0, \qquad 3.$$

$$\text{with} \quad \underline{\underline{g}} = \left(\lambda^2 - \lambda^{-2\nu}\right) \mathbf{nn} + \lambda^{-2\nu} \underline{\underline{\delta}}. \qquad 4.$$

The metric tensor $\underline{\underline{g}} = \underline{\underline{\lambda}}^{\mathrm{T}} \cdot \underline{\underline{\lambda}}$ encodes fractional (squared) changes of lengths, the directions along which are selected out by the $d\mathbf{R}_0$.

If the $\underline{\underline{\lambda}}$ were imposed, then $\underline{\underline{\lambda}}^{\mathrm{T}} \cdot \underline{\underline{\lambda}}$ would be the Cauchy–Green tensor of the distortions in elasticity (24). But here, we are concerned with spontaneous length changes in the plane of an initially flat sheet that will remain our reference state to describe the new surface. The new lengths $|d\mathbf{R}|$ are those natural to the changed state and are effectively stretch free, that is, without stress. We confine ourselves to a planar reference state with $\mathbf{n}$ in-plane, so that the relevant 2×2 part of Equation 2 is simply, in the director frame, $\begin{pmatrix} \lambda^{-\nu} & 0 \\ 0 & \lambda \end{pmatrix}$. With stress-free surfaces, the normal direction will simply relax always by $\lambda^{-\nu}$.

In summary, we have a simple, flat reference plane on which a $\underline{\underline{g}}$ is defined that specifies the target. The challenges are to find the curvature and then ultimately the actual surface. Even more ambitious is the inverse problem: Give the patterns determining a $\underline{\underline{g}}$ that will generate a desired surface. We sketch this program, along with its many, as yet unresolved, challenges.

If $\underline{\underline{g}}$ is independent of position, for instance, if there is a change to $\lambda \neq 1$ but it remains spatially constant, while $\mathbf{n}$ is along a fixed direction, then such a strip, say, would simply get longer or shorter but remain flat. However, if $\underline{\underline{\lambda}}(\mathbf{r})$ and hence $\underline{\underline{g}}(\mathbf{r})$ vary with position $\mathbf{r}$ in the reference plane, then the sheet must develop curvature as $\underline{\underline{\lambda}}$ evolves. This is Gauss's celebrated *Theorema Egregium* that GC is an intrinsic geometric property and is determined by variations of the first fundamental form $\underline{\underline{g}}$. An excellent, elementary discussion of these notions in this context of evolving surfaces is in Reference 25. Also in this context is the review in Reference 26. At this point, we should carefully define intrinsic curvature: A plane that rolls up to a cylinder has suffered bend in one direction—an extrinsic curvature—but distances between points in the original space have not changed. Triangles drawn on the original surface remain triangles in that their sides remain geodesics, that is, the shortest distance between two points (in this case corners of the triangle). Furthermore, the interior angles of the triangle continue to add up to 180°. The curvature is the inverse of the cylinder's radius. In general, it is the inverse of the radius of curvature of a cylinder that can be fitted locally to the surface that we are bending in one direction. In the other direction the cylinder's curvature is zero, so the radius of curvature is infinity.

However, as the map maker well knows, if a plane wraps a sphere, then distances in the plane have to change. Otherwise there are wrinkles or tears. The sphere curves in two directions. The product of the two curvatures at a point is (*a*) nonzero (unlike for the cylinder or for surfaces locally like a cylinder), and (*b*) independent of the two directions we choose to define each of the bends in. It is an intrinsic property of the surface (*Theorema Egregium*). (A sphere is a special case; the intrinsic curvature κ is the same everywhere on its surface and is $\kappa = 1/R^2$, where R is the sphere's radius.) Triangles can be formed on the sphere's surface by connecting three points by geodesics

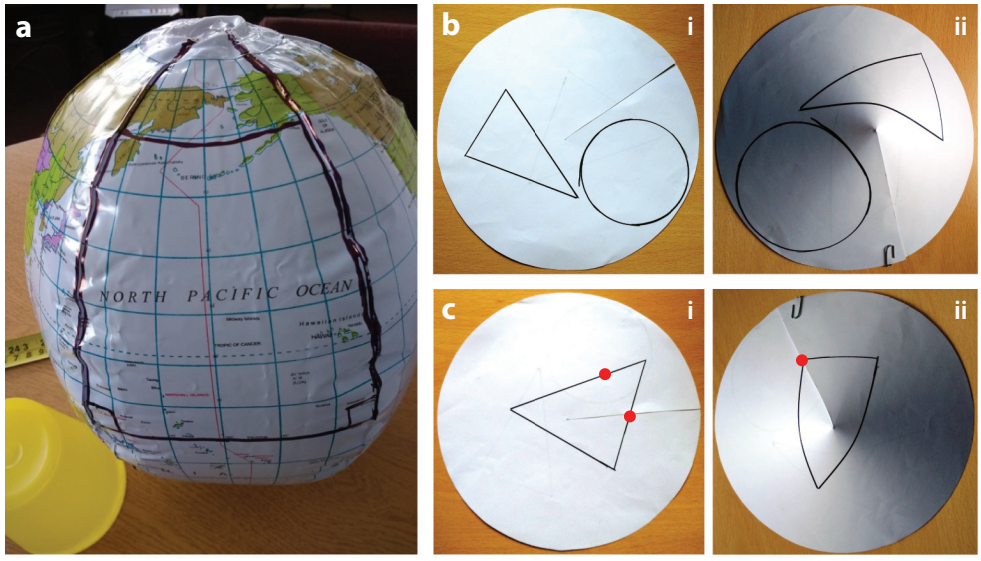

Figure 5

(*a*) Three great circles on a sphere—the shortest distances between pairs of points—form a triangle. Here, the two right-angle interior angles sitting on the Equator account alone for the usual 180°, with additional angle at the North Pole. (*b*, *i*) A disc with a radial cut to its center with a triangle and circle drawn on it. (*b*, *ii*) The edges of the radial cut are swept over each other to give an angular deficit at the center. A cone results. The triangle of the flank remains conventional, with angles adding up to 180°. (*c*, *i*) The disc turned over to show a triangle spanning its center. (*c*, *ii*) The angular deficit is again introduced until the red dots in panel *c* are superposed. In the new triangle, the angles now add up to more than 180° because the cone apex punctures the triangle. Geodesics (for instance the triangle's sides) remain so because the "distortion" is isometric. Clearly Gaussian curvature in cones is localized to the tip (the size of the new triangle does not matter).

(great circles), but as is well known, the sum of the interior angles is greater than 180° by an amount that depends on the enclosed area, i.e., on how big the triangle is (see **Figure 5*a***). If we took a flat sheet with a triangle on it and, by some miracle (to be revealed below!) were to transform it into part of a spherical shell, then the sides of the triangle would no longer all be geodesics; that is, we would no longer have a true triangle. A cone by contrast would appear to lack GC as a cylinder does. It is only bent in one of two directions. There are subtleties, however, and a cone indeed has GC (see **Figure 5*b–c*)**. We now address cones as our first example of topography development.

3.1. Cones from Circular, Radial, and Logarithmic Spiral Director Fields

We illustrate here how reversible topography change arises in simple systems before addressing general problems of curvature creation and its control. Assume in Equation 4 for the metric tensor that λ has no spatial variation, and that variation in $\underline{\underline{\mathbf{g}}}$ is purely due to that of the director $\mathbf{n}(\mathbf{r})$.

Figure 6 shows a director field of concentric circles in a plane disc. It is a 2D version of a +1 liquid crystal disclination. From the figure, one can see that if the disc suffers circumferential contractions and radial elongations, then the ratio of circumference to radius cannot remain 2π. The disc cannot remain planar but becomes a cone, with cone (internal) angle $\phi = \sin^{-1}(\lambda^{1+\nu})$. There is an angular deficit, but unlike in **Figure 5*b–c*** it is achieved by a nonisometric transformation. The illustration with paper discs and cones makes the point about localized GC, but it is a poor analogy for shape-transforming LC mechanics, as we see below for generic geodesics. The

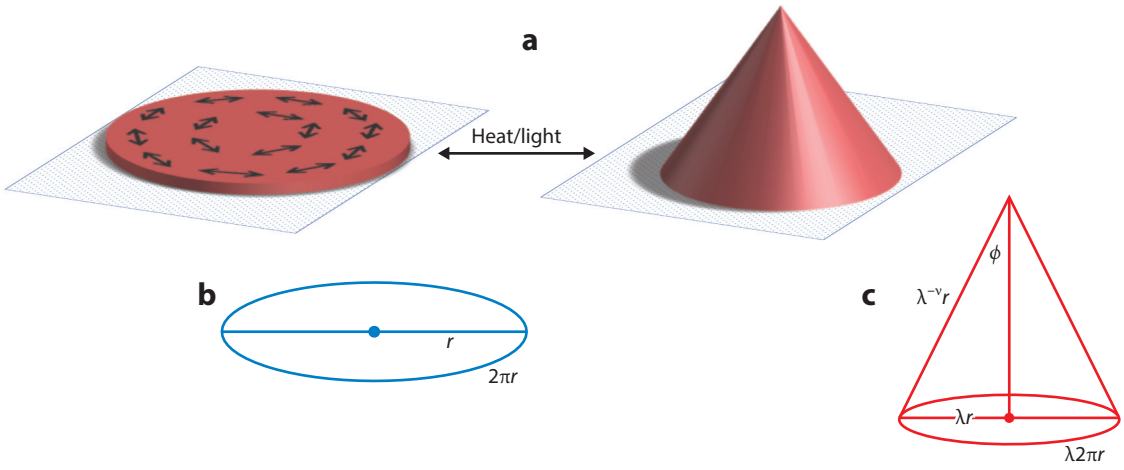

Figure 6

(*a*) A circular director pattern in a flat disc, and the transformation of the disc to a cone as the circumferences contract by $\lambda < 1$ and the radii elongate by $\lambda^{-\nu}$. (*b*) A circle of radius r and circumference $2\pi r$ that will become the base of the cone. (*c*) A cone with side (intrinsic radius) $\lambda^{-\nu} r$ and base of circumference $\lambda 2\pi r$ that is generated by an in-space radius λr. The right triangle gives the cone's internal angle ϕ as $\sin\phi = \lambda^{1+\nu}$.

GC is $\kappa = 2\pi(1 - \sin\phi) = 2\pi(1 - \lambda^{1+2\nu})$. See Modes et al. (27, 28) for LC solid structures, and an important paper by Dervaux & Ben Amar (29) with similar structures in the context of soft tissue morphogenesis. We now describe their realization and application.

3.2. Patterning, Arrays of Cones, and Lifters

The first responsive GC shell was apparently that of Camacho-Lopez et al. (10), the celebrated LCE swimmer "that swims into the dark," a photodriven flapping shell on a fluid surface. The vital step to creating more general metric-mechanical materials is the encoding of the director, from which the pattern of length changes will follow. There exist well-established techniques from LC technology for setting up director fields. Broer et al. and White et al. have perfected their application to the creation of programmed LC solids. Complex patterning in photo-glasses was created by de Haan et al. (30) using photomasks and polarized light to create guide surfaces from photosensitive materials. These form the mold for the liquid that will become the LC solid when polymerized and crosslinked, after the director field has been established by the guide surfaces. Careful registry of the top and bottom surfaces, held apart by a distance that will become the thickness of the LC solid, is required. See Reference 30 for the process and extensive references to earlier literature. The guide surfaces are removed to release the photothermal sheet. De Haan et al. achieved considerable deformations from discs to cones of $\phi = 40^\circ$ internal angle on heating a flat disc with a $+1$ defect at its center. These defects, and also those with a large range of other topological charges, were also encoded by McConney et al. (31), where techniques are further described. See also Ahn et al. (15), in which the angles of cones are measured and compared during relaxation with back isomerization in this photomechanical example. (Note that their cone angle is the complement of our ϕ.)

We now turn to spectacular mechanics applications: White and coworkers have created arrays of $+1$ circular disclination patterns in flat, slender sheets of LC solids that then on (here thermal) activation produce an array of cones that rise out of the plane (32, 33) to achieve their natural, stress-free state. These are very powerful lifters indeed, and we meet for the first time the full

Figure 7

(*a*) 3 × 3 patterns of circular directors lead to (*b*) 3 × 3 arrays of cones rising from the flat square on heating. (*c*) A 2 × 2 array of cones lifts two glass sheets several times its own weight. (*d*) A plastic spoon being pressed on its Gaussian curved region. Radial and circumferential lines of compression and extension, respectively, arise when this curved shell is deformed. Panels *a–c* adapted from Reference 32 with kind permission of Tim White.

force of this metric-shifting mechanics. **Figure 7*a,b*** shows a director patterned sheet before and after heating, giving a 3 × 3 array of cones. In **Figure 7*c***, a 2 × 2 array lifts a load of glass plates. **Figure 7*d*** is a familiar example; one can bend the handle of a plastic spoon, but deforming the Gaussian-curved cup of the spoon is difficult. Force from an applied finger is met by compressive forces radially and extensional forces circumferentially.

Evolving cones, though slender, can be very strong and can lift of order 3,000× their own weight through a distance several times their thickness. **Figure 8** shows a director pattern leading to lifter arrays that can lift the indicated multiple of their own weight. The lifter sheets are 0.2 mm thick and about 1 cm square and are thus slender (a 50:1 lineal dimension/thickness ratio). They lift their loads through a height of between ×8 and ×2 their thickness. See Reference 33 for the loading for optimal work delivery. One also sees no apparent fatigue over many cycles.

Before leaving cones, which arose from +1 defects, we note that other systems (not immediately of apparent mechanical significance) are also possible. De Haan et al. (30) also made sheets with a +1 radial, rather than circumferential, director field. Now on heating or illumination, radii shrink and circumferences develop surplus length. The result is what has been termed (27, 28) an

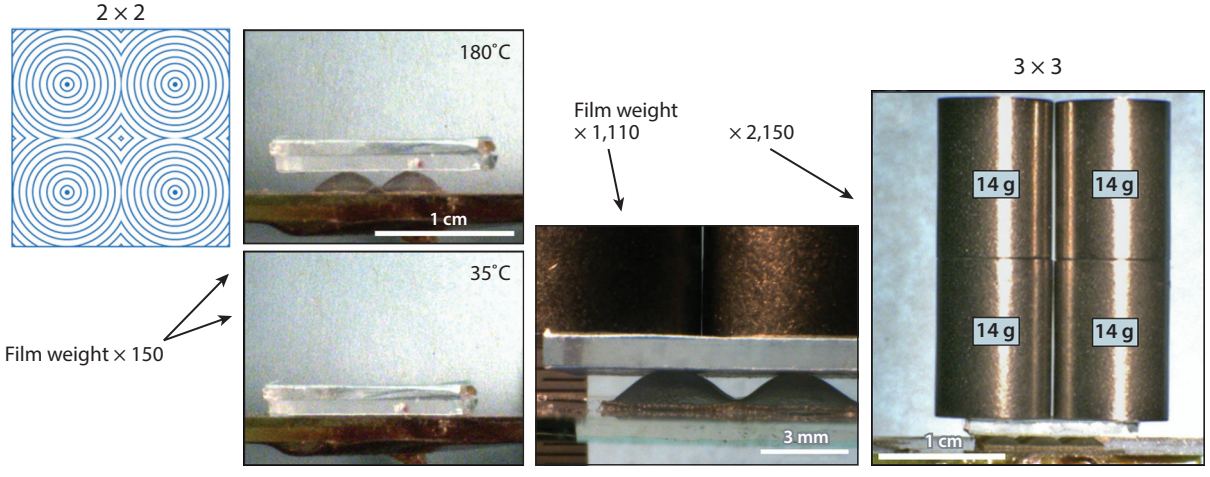

Figure 8

A 2 × 2 pattern of circular directors leads to a 2 × 2 array of cones rising from a flat square when the temperature is raised from 35°C to 180°C. The multiple of the cone array's weight that is being lifted is shown for each example. The ×1,100 array is shown close up. Figure adapted from Reference 33 with kind permission of Tim White (CC-BY 4.0).

anticone, something like a ruff with a wavy perimeter and straight radii. There is negative GC (an angular surplus) at the tip; such structures have been investigated in closely related contexts of morphogenesis and growth (29, 34). McConney et al. (31) also encoded anticones, but went on to explore a large range (extending to ±10) of other topological charges, where even more complex distributions of GC (35) and topography arose. See also Reference 36 for a +6 defect and for a very sharp +1 cone and Ahn et al. (15) for anticones (radial +1 defects) and also −1 charge defects and their mechanical distortions. One can also take analytic expressions (35, 37) for the GC associated with defects and, for $\pm\frac{1}{2}$ defects, numerically compute (38) the emerging shapes. Defect systems have been simulated by Selinger and colleagues (39) who, in addition to exploring cones and saddles, examined exotic systems such as the distortions arising from −2 and −4 defects. In effect, topology leads to photoinduced topography, to paraphrase McConney et al.

4. GAUSSIAN CURVATURE FROM VARYING METRICS

Nature shows us spatially differential growth that leads to complex form. Simplest are perhaps leaves that wrinkle and buckle either in normal growth or as the result of disease. It has motivated many mechanics studies in this context of evolving shells, though as a consequence of a simple $\underline{\underline{\boldsymbol{\lambda}}}(\mathbf{r})$ variation of isotropic growth, that is, without an $\mathbf{n}(\mathbf{r})$ predicating directions of anisotropic transformations (λ and $\lambda^{-\nu}$ in our case). Consequentially, the metric is just $\underline{\underline{\mathbf{g}}} = \lambda^2(\mathbf{r})\underline{\underline{\boldsymbol{\delta}}}$—a local inflation or deflation. The basic ideas required for a study of (reversible) LC solid transformations are established in such studies of locally isotropic swelling, and many interesting 3D structures are obtained experimentally too. See the comprehensive theory (40) and the reviews (25, 41) of the geometry and of important experimental results. See earlier papers (29, 42–44), and subsequently Kim et al. (45) also on programmable differential swelling in gels creating intrinsically curved topographies.

We now concentrate on circularly symmetric, homogeneous λ systems, that is, where the only variation in $\underline{\underline{\boldsymbol{\lambda}}}$, and hence in $\underline{\underline{\mathbf{g}}}$, is through $\mathbf{n}(r)$, that is, where the director varies as in **Figure 9**. For circular symmetry, the director makes an angle $\alpha(r)$ with the radial direction depending only on the magnitude r. The cases $\alpha = \pi/2$ and $\alpha = 0$ are the circular and radial director fields, respectively, of the previous examples. The first experimental realizations of the shells we discuss below have been from the White group (46). We sketch a mathematical machinery (37, 46–48), not pursuing Cartesian patterns of $\mathbf{n}$ also used to generate these circularly symmetric shells (37, 46, 47).

In Cartesian coordinates, the reference state increment $\mathrm{d}\mathbf{R}_0 = (\mathrm{d}x_0, \mathrm{d}y_0)$ becomes in circular polar coordinates $(\mathrm{d}r, \mathrm{d}\theta)$. For the former, the metric is $\left(\begin{smallmatrix}1 & 0\\ 0 & 1\end{smallmatrix}\right)$, whereas to get the correct length $|\mathrm{d}\mathbf{R}_0|^2 = (\mathrm{d}r)^2 + r^2(\mathrm{d}\theta)^2 \equiv (\mathrm{d}r, \mathrm{d}\theta)\cdot\underline{\underline{\mathbf{g}}}\cdot(\mathrm{d}r, \mathrm{d}\theta)$ (see **Figure 9*a***), the metric transforms to $\left(\begin{smallmatrix}1 & 0\\ 0 & r^2\end{smallmatrix}\right)$. On deformation by $\underline{\underline{\boldsymbol{\lambda}}}$, Equation 2 with $\mathbf{n}$ as above, the squared lengths in the target space in terms of a reference space $(\mathrm{d}r, \mathrm{d}\theta)$ are given by the metric (46),

$$\begin{aligned} g_{rr} &= \lambda^2 + \left(\lambda^{-2\nu} - \lambda^2\right)\sin^2(\alpha),\\ g_{r\theta} = g_{\theta r} &= \tfrac{1}{2}r\left(\lambda^{-2\nu} - \lambda^2\right)\sin(2\alpha),\\ g_{\theta\theta} &= r^2\left[\lambda^{-2\nu} - \left(\lambda^{-2\nu} - \lambda^2\right)\sin^2(\alpha)\right]. \end{aligned} \qquad 5.$$

Curves with a (unit speed) parameterization via arc length s have $\mathbf{r} = (r(s), \theta(s))$. Their tangent vector is $\mathbf{t} = \mathrm{d}\mathbf{r}/\mathrm{d}s = (\dot{r}(s), \dot{\theta}(s))$ that is a unit vector (with the above $\underline{\underline{\mathbf{g}}}$) in the reference state because $|\mathbf{dr}| = \mathrm{d}s$ (see **Figure 9*a***). The tangent vector transforms to a $\mathbf{t}' = \underline{\underline{\boldsymbol{\lambda}}}\cdot\mathbf{t}$ with new length $|\mathbf{t}'|^2 = \mathbf{t}'\cdot\mathbf{t}' = \mathbf{t}\cdot\underline{\underline{\mathbf{g}}}\cdot\mathbf{t}$. As one sees in **Figure 9**, curves are in general changed in length, rotated,

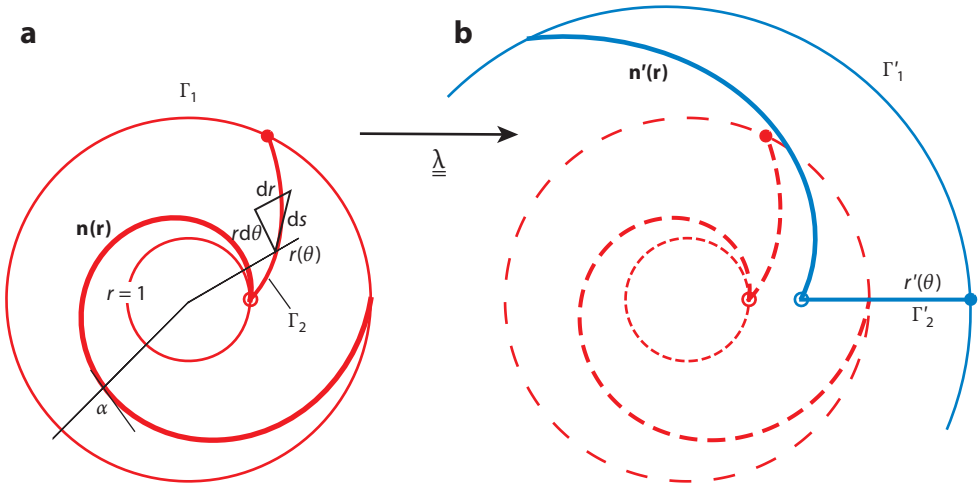

Figure 9

(*a*) A disc of liquid crystalline solid before deformation, showing a unit circle and an outer circle Γ_1. A director line $\mathbf{n}(\mathbf{r})$ (*heavy line*) spirals outward with angle $\alpha(r)$ to radii. A material curve $r(\theta)$ marked Γ_2, which turns out to be a protoradius, has differential length components $r\mathrm{d}\theta$ and $\mathrm{d}r$ in the θ and r directions that make up a length $\mathrm{d}s$. (*b*) The intrinsic curves after transformation by $\underline{\underline{\lambda}}(\mathbf{r})$ showing an inflated circle Γ'_1, the radial image Γ'_2 of the protoradius, and the convected and rotated final director field $\mathbf{n}'(\mathbf{r})$.

and convected [see Mostajeran et al. (49) for a discussion of these effects of $\underline{\underline{\lambda}}$]. An example is $\mathbf{t}_1 = (0, 1)$, the tangent to a circumference, Γ_1. Employing Equation 5, on transformation of $\Gamma_1 \to \Gamma'_1$, the circumference changes in length by a factor of $\sqrt{g_{\theta\theta}/r^2}$ (see Equation 8).

Target space radii, that is, curves Γ'_2 that are perpendicular to circumferences, are more subtle to determine: Because of rotations of their tangents, $\mathbf{t}_2$ say, they start as reference state protoradii, Γ_2 in **Figure 9*a*** that evolve under $\underline{\underline{\lambda}}$ to actual radii, Γ'_2. One shows (48) from Γ'_2 being perpendicular to Γ'_1, that a protoradius $r(\theta)$ satisfies a simple ordinary differential equation (ODE):

$$\mathrm{d}r/\mathrm{d}\theta = -g_{\theta\theta}/g_{\theta r} \quad \to \quad \theta = -\int \mathrm{d}r g_{\theta r}/g_{\theta\theta}, \qquad 6.$$

giving a single quadrature for r because the ODE's right-hand side is independent of θ.

An example is where α is independent of r; that is, lines of $\mathbf{n}$ are log spirals: $r_n(\theta) = r_{n0}\mathrm{e}^{b\theta}$ with $b = \cot\alpha$. Also, the integrand in Equation 6 is $g_{\theta r}/g_{\theta\theta} \propto 1/r$, whence the protoradius is simply $r(\theta) = r_0\mathrm{e}^{c\theta}$, where $c = \cot\beta$, with β being the (constant) angle between the tangent of $r(\theta)$ and a radius. It is thus also a log spiral, with c dependent on the elements of $\underline{\underline{\mathbf{g}}}$, that is, on λ and α (see References 27, 28, 49). The factors by which circumferences and radii change are independent of r, and we again have cones or anticones. The differences from our earlier cones are the rich rotations, convections, and distortions. For instance, Γ'_2 is a geodesic, but its source Γ_2 is not. The paper cone model of **Figure 5*b–c***, and used by this author in lecture demonstrations, is a deeply misleading illustration of the nonisometric transformations of LC solids. Triangles do not remain triangles because generally geodesics do not remain so after deformations $\underline{\underline{\lambda}}$. However, the paper demonstration of localized GC remains relevant. See Reference 49 for a full discussion of geodesics for these solids.

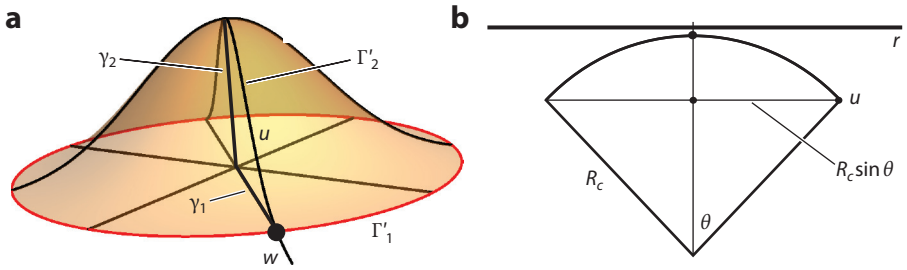

Figure 10

(*a*) A point *w* (*heavy dot*) in the cylindrically symmetric surface is specified by the radius $\gamma_1(u)$ and the height function $\gamma_2(u)$, both of which are functions of the in-surface radius' (Γ_1') length $u(r)$ from the apex. The transformed circumference of $\Gamma_1' \equiv 2\pi\gamma_1$ is a known multiple, $\sqrt{g_{\theta\theta}/r^2}$, of the original ($\Gamma_1$) circle's circumference, $2\pi r$. (*b*) A disc deforms to a spherical cap, seen in section, with the initial radius r becoming the intrinsic radius u.

4.1. The Forward Problem: From Directors to Shells

Three elements (48) take one from a director field to a shell:

1. The GC arising from λ and the $\alpha(r)$ obtain from the spatial variation of $\underline{\underline{\mathbf{g}}}$:

$$K(r) = \frac{\lambda^{-2} - \lambda^{2\nu}}{2}\left[\left(\alpha'' + \frac{3}{r}\alpha'\right)\sin(2\alpha) + 2\alpha'^2\cos(2\alpha)\right], \qquad 7.$$

   a function of the reference coordinate r, here through $\alpha(r)$, and α' is $\mathrm{d}\alpha(r)/\mathrm{d}r$.
2. A symmetric shell can be specified in the target space by radius and height functions, γ_1 and γ_2, functions of the in-material (intrinsic) radius, u. See **Figure 10*a***. Smooth shells also have $\gamma_1'^2 + \gamma_2'^2 = 1$, where $' = \mathrm{d}/\mathrm{d}u$, so γ_1 and γ_2 constrain each other. The GC is $K = -\gamma_1''/\gamma_1$, with the constraint making this expression less simple than it seems. It is in terms of u, not r as in Equation 7.
3. One needs to connect the reference and target radii r and u, which can be achieved via the arc length expression: $\mathrm{d}u = \mathrm{d}s\sqrt{\mathbf{t}_2 \cdot \underline{\underline{\mathbf{g}}} \cdot \mathbf{t}_2}$. The $\mathrm{d}s$ can be replaced by $\mathrm{d}r$ by taking $\mathrm{d}r/\mathrm{d}s$ out of the surd and replacing remaining $\mathrm{d}r/\mathrm{d}\theta$ terms in the surd by its form in Equation 6 for protoradii.

   Another reference/target connection is circumferential inflation, $\Gamma_1 \to \Gamma_1'$, that is,

$$2\pi r \to 2\pi\sqrt{g_{\theta\theta}(r)} = 2\pi\gamma_1, \qquad 8.$$

   because the in-space radius γ_1 sweeps out Γ_1'.

An example director field is that specified by $\alpha(r) = \alpha_0 + r^2$, which leads to the GC and shell shown in **Figure 11**. Radial positions r are here scaled by the disc radius.

For many applications of shells, it is useful to anchor them to passive substrates at some circumference with radial position r in the reference state. It is only possible to develop a shell and to remain fixed to the substrate if the circumferences match, that is, $2\pi\gamma_1 = 2\pi r$. It will only be possible at values of λ such that $g_{\theta\theta} = r^2$. For other values of λ there are stretches required to make the two regions compatible at r, and it is likely that shells are inhibited until they snap into place as λ approaches the required value at r. The other requirement is that $\nu > 1$, so that the area of the formed shell can be greater than that of the original disc; this is clearly required if the shell is

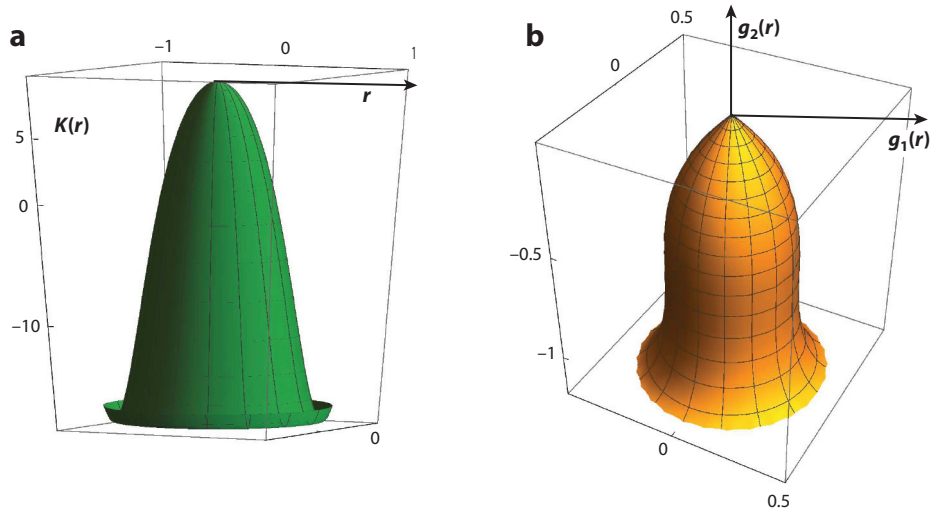

Figure 11

(*a*) Calculated GC and (*b*) shell shape arising from a deformation, $\lambda = 0.51$ and $\nu = 1.5$, in a spatially varying director field $\alpha(r) = \alpha_0 + r^2$, with $\alpha_0 = 1.25$. The GC is plotted against the radial coordinate r of the initially flat, undistorted reference state. The shell is plotted parametrically with r specifying the radial coordinate $g_1(r) \equiv \gamma_1[u(r)]$ and the height function $g_2(r) \equiv \gamma_2[u(r)]$. Both plots correspond to the same region $r \in [0, 1]$ of the reference state. Abbreviation: GC, Gaussian curvature.

to rise up but with a fixed perimeter. We speculate that for required sudden action, for instance, the pumping of analyte in microdiagnostics, the timing of which is critical, these systems could be important.

4.2. The Inverse Problem: From Shells to Directors

We now depart from the forward problem [where, given **n(r)** we calculate the shell shape resulting from the action of heat or light]. The inverse problem is, given a shell, what director field **n(r)** must we program to achieve this shape under the action of heat and light? These inverse problems are of various types.

4.2.1. Cylindrical symmetry. The inverse problem for anisotropic solids has been attacked by Aharoni et al. (37) and Mostajeran et al. (46, 48). The simplest problem is that of constant GC, that is, for spherical caps and spindles[2] ($K > 0$) and hyperbolic spheres ($K < 0$). Then Equation 7 for K is a simple ODE for $\alpha(r)$ with solution (46)

$$\alpha(r) = \pm\tfrac{1}{2}\arccos\left[-\tfrac{1}{2}C(K)\,r^2 + c_1 + \frac{c_2}{r^2}\right], \qquad 9.$$

where $C(K) = K/(\lambda^{-2} - \lambda^{2\nu})$, and c_1 and c_2 are real constants of integration. Depending on c_1 and c_2, one has simple discs or annular domains. For instance, if $K > 0$, $c_2 = 0$, and $c_1 \leq 1$, the solution (Equation 9) defines a spiral pattern on the simple disc $r \leq \sqrt{\frac{2(1+c_1)}{C(K)}}$. Kowalski et al. (50) have measured the thermal response of discs with director spirals from the family of Equation 9 (see **Figure 12*a–f***showing spherical caps and spindles, and hyperbolic spindles). This work also

[2]Spherical spindles have curvatures differing in the two principle directions such that their product, the GC, is constant. They have peaks at their pole, unlike spherical caps.

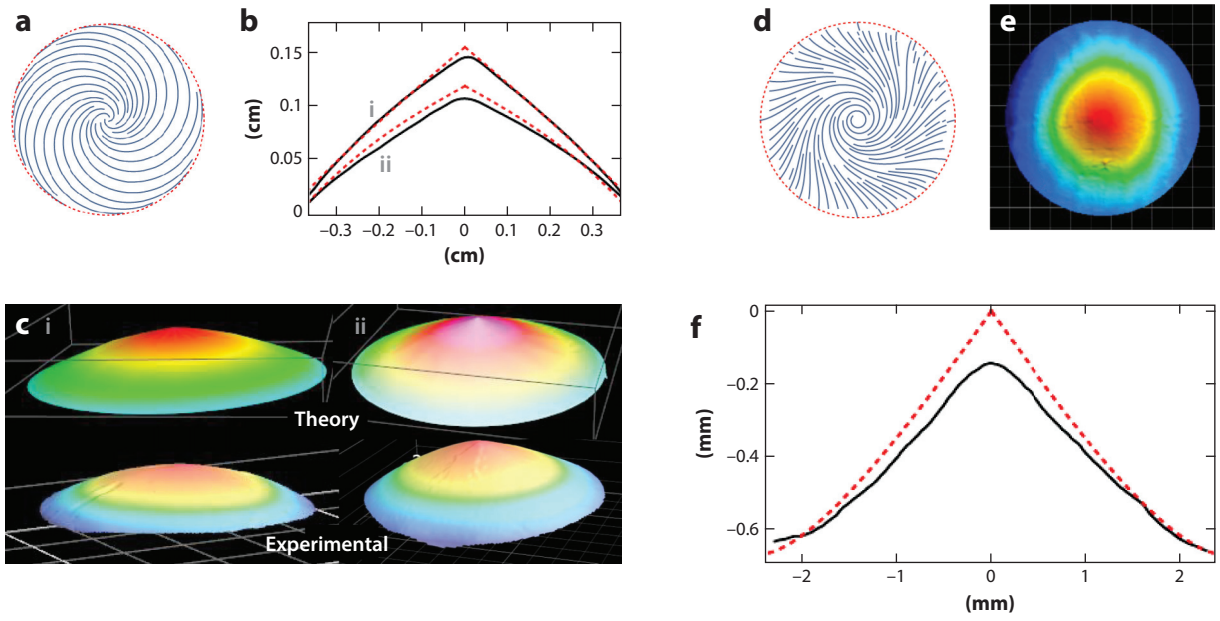

Figure 12

Constant GC upon heating. Positive GC: (*a*) Spiral director profile with $c_1 = -0.35$. (*b*) Predicted and measured height profiles for $c_1 =$ (*i*) -0.75 and (*ii*) -0.35, showing fine control over curvature. (*c*) Predicted and measured 3D shapes for *i* (*right*) and *ii* (*left*). Negative GC: (*d*) spiral with $c_1 = -1$, (*e*) measured height profile for the expected hyperbolic spindle, and (*f*) representative radial slice through the shell, showing good agreement between the predicted (*dashed*) and measured (*solid*) profiles. Abbreviation: GC, Gaussian curvature. Figure adapted from Reference 50.

presents circumferentially anchored spherical caps as an example of integration of responsive shells with passive supports. Thicker, complex, responsive shells can be 4D printed (51–53). LC polymers align during extrusion from the printing head. Printing is 4D because 3D-printed structures subsequently morph, as above.

In general, the inverse problem is rather difficult (37, 48), even for these systems of circular symmetry. The problem is that defining the desired surface gives the GC in terms of the equivalents of the γ_is and the target space radius u, whereas the director field in terms of $\alpha(r)$ is in the reference state. Making the connection in general involves integral equations (48), but two important cases allow for analytical solutions—paraboloids and catenoids of revolution. In these cases, for a given target shell achieved at a deformation $\lambda = \Lambda$, the required director pattern is characterized by an $\alpha_\Lambda(r)$ field that is unique to that particular Λ. This must be written into the initially flat disc. A consequence is that, as heating or illumination proceeds, λ does not immediately attain the Λ value. Intermediate shells are created on the way to Λ that are not of the desired form. For instance, before a required paraboloid is attained, there will be shell conformations that are peaked at their pole (see Reference 48 for explicit details).

4.2.2. Beyond circular symmetry. More general and powerful machinery is required to deliver intrinsic curvature leading to noncircularly symmetric shells. It is a difficult problem, meriting a review in itself. However, see Plucinsky et al. (54), who allowed director rotation out of plane and gave a precise specification of the director field in terms of gradients of the lift required out of the plane to specify a (general) shell. Further, Aharoni et al. (55) developed numerical schemes to specify patterns leading to nonsymmetric shells. Griniasty et al. (56) recently showed that the

inverse problem is locally solvable for any 2D geometry about any point. They also show there is a continuum of director fields that give the same intrinsic geometry; see below, however, for going beyond intrinsic questions.

5. THE GRAND CHALLENGE: RELATED SYSTEMS

5.1. Control of Intrinsic Curvature and Extrinsic Bends: The Challenge of Complete Topography Control

We have been concerned with creating a metric and thus the intrinsic (Gaussian) curvature, leaving open the question of extrinsic curvatures (simple bends) of the plane. The product of the curvatures, $\frac{1}{R_1} \times \frac{1}{R_2}$, is the GC and is intrinsic to the surface. We have discussed above evolved shapes that are without stretch, paying no regard to the bend cost, which is much smaller than stretch cost when systems are thin. However, for arbitrary surfaces, one needs to generate both the required GC and the mean curvature, that is, the two invariants of the surface. This very ambitious program of inverse, general surface problems has been addressed by various authors (37, 55, 57). There are varying strategies for controlling extrinsic curvature, for instance, out of plane variation of director through the thickness or anisotropic swelling by an amount differing through the thickness. Metric changes are determined by the contraction/elongation averaged through the thickness, with deviations from the average determining choices of bends with associated elastic costs. Alternatively, director variation can remain in-plane but in directions that vary through the thickness. Director deviation from the mean by twist through the thickness then gives negative GC (saddle-like) deviation from the GC implied by the in-plane spatial variation of the mean director. Progress has been striking and has yielded, for instance, faces that evolve from flat sheets (55, 58). Similarly, the evolution of a calla lily flower (57) has been achieved from a flat sheet of hydrogel where swelling is rendered anisotropic by the embedding of aligned stiff fibers. Full implementation of this program will achieve a complete solution of topography evolution and control.

5.2. Related Systems and Phenomena

A wide range of systems exhibit topography change on various forms of actuation. They have a formal similarity with the systems we have described, and the same geometrical and mechanical methods we have developed can be used to model them.

5.2.1. Baromorphs. Siéfert et al. (58) turned to a different route to mechanical actuation—applying pneumatic pressure to channels in elastomer sheets: when under pressure, the channels expand perpendicular to their long axis, while remaining unchanged in length. In our notation, there is an elongation λ along a director which is in-plane and perpendicular to the channels. Since lengths in the channel direction are unchanged, then the "pneumatic Poisson ratio" for this direction is $\nu = 0$. Pressure controls the magnitude of λ, and dynamics can be pursued by varying the pressure. Furthermore, the authors have control over the channel patterns and can create shapes at will that they term "baromorphs." See, for instance, **Figure 13**. The authors have made not only more complex shapes than cones, such as anticones, caps, etc. (58), but also faces as in Section 5.1. Furthermore, they have new methods (E. Siéfert, E. Reyssat, J. Bico, and B. Roman, private communication) to make very large, rigid, and light shape-morphing shells that will undoubtedly find new applications in the macroscopic realm.

Another very recent paper also engineers spatially dependent deformations in conventional elastomers, but instead uses electric fields that give spatially dependent Maxwell squeezing stresses

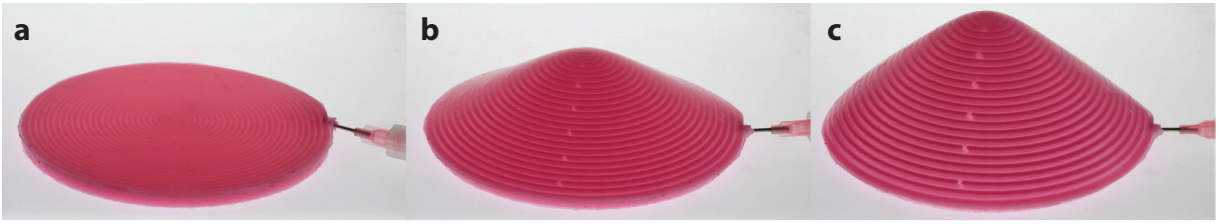

Figure 13

Baromorphs with concentric circular channels: (*a*) uninflated and hence flat. (*b*) Partially inflated. (*c*) Strongly inflated to form a pronounced cone. Photos provided by E. Siéfert et al.; see Reference 58 for more examples.

(59). Internal distributions of electrodes, analogous to the channels of baromorphs, give isotropic in-plane elongations depending on the local field. However, because these elastomers are mechanically homogeneous and isotropic, several independent shapes could be made on the same elastomer volume using separate sets of internal electrodes as required. The results are caps, saddles, and sections of tori, with the solution of the inverse problem (Sections 4.2, 5.1, and 5.2.2) required for more complex shapes.

5.2.2. Topography change of inked plastic sheets. We have seen there is an extensive literature on achieving Gaussian curved shells by the spatial control of the extent of locally isotropic swelling [see the review by Sharon & Efrati (41) and the subsequent work of Kim et al. (45), where programming and encoding response in 3D has been achieved]. As an example of these ideas applied to very different systems, recently Mailen et al. (60) have used biaxially prestretched plastic sheets to produce GC shells. Contraction, locally isotropic in the plane, can be photoinduced to partially recover the state before stretching. The local extent of recovery, that is of contraction, is determined by the optical density of ink at that point and, hence, the extent to which heat is produced. Thus, one can print plastic sheets with an ink intensity that encodes the spatially varying metric change.

For the thin sheets of Mailen et al., the considerations are purely geometric because bend is much cheaper than stretch, the lack of which will select out the desired symmetric shell shape. The authors aimed for spherical caps, a problem addressed by Kim et al. (45) using metric methods. A very simple argument (61) specifies the required pattern of contractions to yield a spherical cap. It relies on mappings from r to u sketched in **Figure 10*b***. Both methods yield contractions varying on the initial disc (r) like

$$\lambda(r) = \frac{\lambda(0)}{1 + \left(\frac{\lambda(0)}{2}\right)^2 (r/R_c)^2}, \qquad 10.$$

where R_c is the radius of curvature of the cap, and $\lambda(0)$ is the contraction at the center of the disc. Furthermore, their inverse problem has also been solved more generally (61), getting beyond spheres and saddles, and concrete examples, e.g., paraboloids and catenoids, have been given too. Thermoplastics have also recently been printed with a preferred (extrusion) direction, leading to directional shrinkage and shell formation on heating (62).

5.2.3. Reprogrammable and autonomous shells. Another ambitious direction in which there has been recent progress is that by Priimägi and colleagues (63–66) in making self-regulating, autonomous and reprogrammable shells. Although these various shells are not Gaussian curved, they

bend in ways that point to future responsiveness and functionality, for instance, in reprogrammable soft robots that learn from their environment and past actions.

A self-regulating iris (63) is open in the dark state, having curled back the segments attached at a perimeter that then unroll in the light and close off a circular iris. The light being admitted is automatically regulated. Greater sensitivity to light intensity of the mechanical response is achieved by polymerizing close to the nematic–isotropic transition, a strategy that will be useful elsewhere too: Weaker nematic order is imprinted on the solid, and hence the disturbance created by the light need not be so great to lower the order.

An optical bender that is open when unilluminated can bend when light is reflected from a target object onto its surface that is to become concave (64). It was found that a strong, self-regulating gripper (an artificial fly trap) reacted in 200 ms to the presence of a target it had distinguished from other objects.

Another aim is flexibility and adaptability of function of a shell (65). Having had imprinted at fabrication an underlying functionality, a shell can subsequently be reprogrammed to behave differently, despite receiving the same stimulus, e.g., the same light field. One route to this end has been a synergy between photochemical response (for shape programming) and photothermal response (for shape morphing). It is found that in photochemically modified regions (where UV exposure has produced significant *cis* concentrations of dye) subsequent irradiation with red light, producing heat, causes much greater deformation than if the region is not prepared by UV. The photochemical modifications are long-lived compared with the thermal response to red light (30 min compared with 2 s after respective stimuli cease). Thus, an underlying director field can be temporarily reprogrammed, at least in the magnitude of its response, and a different robotic function achieved. As an example, a gripper (holding 100× its own weight) will grip on red illumination and subsequently either release or hold its load after illumination ceases, depending on how it was prepared. Erasure with blue light returns the *cis* dye isomers to their *trans* state and, hence, the actuator to its original state. Two colors of light and two forms of reaction are perhaps a form of multistimuli action. Rather more literal has been the combination of water vapor and light in a humidity-gated photoactuator (66). Under humid conditions, photoresponse can be engineered to be more efficient, leading to differing actuation under wet and dry conditions—an artificial nocturnal flower!

5.2.4. Shells with discrete distributions of Gaussian curvature: Nonisometric origami.

Classical origami creates facetted versions of cones by valley and mountain folds that meet at vertices where there are angular deficits, and thus localized sources of GC, as we have seen in cones. Paper is magicked away behind folds, and the distortions are locally isometric—the sides of triangles on facets remain geodesics, and the sum of interior angles remains 180°. See the discussion of, and around, **Figure 5*b–c***. But the structures are weak in that they rely on bend (at the folds), which is weak, and which unbend to reveal the lost paper should the structure be loaded. (An exceptional rising hybrid Kirigami–Origami structure from light card (67) supports a colossal load-to-weight ratio of order 10,000.)

Curvature localized at points created by length changes $\underline{\underline{\lambda}}$, varying discretely from region to region of an initially flat sheet, gives an entirely different form of origami. Provided the distortions in neighboring regions are compatible with each other, these regions will become the facets about a vertex in which there is a resulting angular deficit or excess (26, 35, 54, 68). There are strict rules for how neighboring domains can deform (35, 54), and the latter authors coined the apt name "nonisometric origami" for such systems. Very large-scale, nonisometric systems that evolve to facetted shapes have recently been realized (E. Siéfert, E. Reyssat, J. Bico, and B. Roman, private communication).

SUMMARY POINTS

1. We have reviewed mechanics that arise from the manipulation of the metric of a shell, that is, the modification of distances between points, to achieve changes in Gaussian curvature despite the shell remaining stretch free. The motivation is to achieve push and pull in slender systems that would otherwise suffer mechanical instabilities if heavily loaded.
2. This program rests on materials that will respond with large, anisotropic length changes to a range of stimuli. We have reviewed heat, light, solvent, and humidity-driven systems. Our principal concern was liquid crystalline solids, glasses, and elastomers, where the spatial variation of the mechanical response to stimuli was fashioned by the spatial variation of the director, the anisotropy direction, which is imprinted at fabrication.
3. Spectacular lifters have been made, and these offer hope for complex machines at the microlevel, where the functionality arises from the material itself. Ultimately, an aim is to make these responsive machines autonomous and reprogrammable, and important steps have been taken along this route.
4. The grand challenge is of complete control over topography, beyond the symmetric examples we have largely focused on. Considerable progress has been made in this difficult problem.

FUTURE ISSUES

1. Applications should now follow from the mechanics principles established in metric manipulation. These involve integrating active, ideally light-driven, elements into complex systems, for instance, large-scale microfluidics. Demonstrated responsive lifters, snappers, and shells with preform should be ideal for a range of applications including haptics, adaptive and reprogrammable surfaces, and microactuation. Multistimuli and self-regulating systems need continuing development, for instance, in curved systems and where load could feed back to control.
2. The grand challenge of controlling both Gaussian and mean curvature needs further concrete implementation both theoretically and experimentally where questions of fidelity and resolution still arise.
3. Nonisometric origami is under investigation, e.g., nonisometric equivalents of more complex origami; curved-fold systems are an example.

DISCLOSURE STATEMENT

The author is not aware of any affiliations, memberships, funding, or financial holdings that might be perceived as affecting the objectivity of this review.

ACKNOWLEDGMENTS

The author acknowledges funding from the Engineering and Physical Sciences Research Council, United Kingdom.

LITERATURE CITED

1. Bhattacharya K, James RD. 2005. *Science* 307:53–54
2. White TJ, Broer DJ. 2015. *Nat. Mater.* 14:1087–98
3. Warner M, Terentjev EM. 2007. *Liquid Crystal Elastomers*, Vol. 120. Oxford, UK: Oxford Univ. Press. Paperback ed. **https://global.oup.com/academic/product/liquid-crystal-elastomers-9780199214860?lang=en&cc=gb#**
4. Warner M, Terentjev EM. 2007. See Reference 3, pp. 1–8
5. van Oosten CL, Harris KD, Bastiaansen C, Broer DJ. 2007. *Eur. Phys. J. E* 23:329–36
6. Liu D, Broer DJ. 2015. *Nat. Commun.* 8:8334
7. Finkelmann H, Nishikawa E, Pereira GG, Warner M. 2001. *Phys. Rev. Lett.* 87:015501
8. Hogan PM, Tajbakhsh AR, Terentjev EM. 2002. *Phys. Rev. E* 65:041720
9. Cviklinski J, Tajbakhsh AR, Terentjev EM. 2002. *Eur. Phys. J. E* 9:427–34
10. Camacho-Lopez M, Finkelmann H, Palffy-Muhoray P, Shelley M. 2004. *Nat. Mater.* 3:307–10
11. Yu Y, Nakano M, Ikeda T. 2003. *Nature* 425:145
12. Harris KD, Cuypers R, Scheibe P, van Oosten CL, Bastiaansen CWM, et al. 2005. *J. Mat. Chem.* 15:5043–48
13. White TJ, ed. 2017. *Photomechanical Materials, Composites, and Systems: Wireless Transduction of Light Into Work*. Hoboken, NJ: John Wiley & Sons. 1st ed.
14. Harvey CLM, Terentjev EM. 2007. *Eur. Phys. J. E* 23:185–89
15. Ahn SK, Ware TH, Lee KM, Tondiglia VP, White TJ. 2016. *Adv. Funct. Mater.* 26:5819–26
16. Corbett D, Warner M. 2007. *Phys. Rev. Lett.* 99:174302
17. White T, Serak S, Tabiryan N, Vaia R, Bunning T. 2009. *J. Mater. Chem.* 19:1045–192
18. Wang DH, Lee KM, Yu Z, Koerner H, Vaia RA, et al. 2011. *Macromolecules* 44:3840–46
19. Lee KM, White TJ. 2012. *Macromolecules* 45:7163–70
20. Dawson NJ, Kuzyk MG, Neal J, Luchette P, Palffy-Muhoray P. 2011. *J. Opt. Soc. Am. B* 28:1916–21
21. Dawson NJ, Kuzyk MG, Neal J, Luchette P, Palffy-Muhoray P. 2011. *J. Opt. Soc. Am. B* 28:2134–41
22. Liu D, Bastiaansen C, den Toonder JMJ, Broer DJ. 2012. *Macromolecules* 45:8005–12
23. Liu D, Broer D. 2017. In *Photomechanical Materials, Composites, and Systems: Wireless Transduction of Light into Work*, ed. TJ White, pp. 303–26. Hoboken, NJ: John Wiley & Sons
24. Atkins R, Fox N. 1980. *An Introduction to the Theory of Elasticity*. London: Longman
25. Marder M, Deegan R, Sharon E. 2007. *Phys. Today* 60:33–38
26. Modes C, Warner M. 2016. *Phys. Today* 69:32–38
27. Modes CD, Bhattacharya K, Warner M. 2010. *Phys. Rev. E* 81:060701(R)
28. Modes C, Bhattacharya K, Warner M. 2011. *Proc. R. Soc. A: Math. Phys. Eng. Sci.* 467:1121–40
29. Dervaux J, Ben Amar M. 2008. *Phys. Rev. Lett.* 101:068101
30. de Haan LT, Sánchez-Somolinos C, Bastiaansen CM, Schenning AP, Broer DJ. 2012. *Angew. Chem. Int. Ed.* 51:12469–72
31. McConney ME, Martinez A, Tondiglia VP, Lee KM, Langley D, et al. 2013. *Adv. Mater.* 25:5880–85
32. Ware TH, McConney ME, Wie JJ, Tondiglia VP, White TJ. 2015. *Science* 347:982–84
33. Guin TH, Settle MJ, Kowalski BA, Auguste AD, Beblo RV, et al. 2019. *Nat. Commun.* 9:2531 **https://creativecommons.org/licenses/by/4.0/**
34. Muller M, Ben Amar M, Guven J. 2008. *Phys. Rev. Lett.* 101:156104
35. Modes CD, Warner M. 2011. *Phys. Rev. E* 84:021711
36. Ware TH, Perry ZP, Middleton CM, Iacono ST, White TJ. 2015. *ACS Macro Lett.* 4:942–46
37. Aharoni H, Sharon E, Kupferman R. 2014. *Phys. Rev. Lett.* 113:257801
38. Zakharov AP, Pismen LM. 2015. *Eur. Phys. J. E* 38:75
39. Konya A, Gimenez-Pinto V, Selinger RLB. 2016. *Front. Mater.* 3:24:1–7
40. Efrati E, Sharon E, Kupferman R. 2009. *J. Mech. Phys. Solids* 57:762–75
41. Sharon E, Efrati E. 2010. *Soft Matter* 6:5693–704
42. Sharon E, Roman B, Marder M, Shin GS, Swinney HL. 2002. *Nature* 419:579–80
43. Klein Y, Efrati E, Sharon E. 2007. *Science* 315:1116–20

44. Sharon E, Roman B, Swinney HL. 2007. *Phys. Rev. E: Stat., Nonlinear, Soft Matter Phys.* 75:046211
45. Kim J, Hanna JA, Byun M, Santangelo CD, Hayward RC. 2012. *Science* 335:1201–5
46. Mostajeran C, Warner M, Ware TH, White TJ. 2016. *Proc. R. Soc. A: Math. Phys. Eng. Sci.* 472:20160112
47. Mostajeran C. 2015. *Phys. Rev. E* 91:062405
48. Warner M, Mostajeran C. 2018. *Proc. R. Soc. A: Math. Phys. Eng. Sci.* 474:20170566
49. Mostajeran C, Warner M, Modes CD. 2017. *Soft Matter* 13:8858–63
50. Kowalski BA, Mostajeran C, Godman N, Warner M, White TJ. 2018. *Phys. Rev. E* 97:012504
51. Ambulo CP, Burroughs JJ, Boothby JM, Kim H, Shankar MR, Ware TH. 2017. *Appl. Mater. Interfaces* 9:37332–39
52. López-Valdeolivas M, Liu D, Broer DJ, Sánchez-Somolinos. 2018. *Macromol. Rapid Commun.* 39:1700710
53. Kotikian A, Truby RL, Boley JW, White TJ, Lewis JA. 2018. *Adv. Mater.* 30:1706164
54. Plucinsky P, Lemm M, Bhattacharya K. 2016. *Phys. Rev. E* 94:010701(R)
55. Aharoni H, Xia Y, Zhang X, Kamien RD, Yang S. 2018. *PNAS* 115:7206–11
56. Griniasty I, Aharoni H, Efrati E. 2019. *Phys. Rev. Lett.* 123:127801
57. Gladman SA, Matsumoto EA, Nuzzo RG, Mahadevan L, Lewis JA. 2016. *Nat. Mater.* 15:413–19
58. Siéfert E, Reyssat E, Bico J, Roman B. 2019. *Nat. Mater.* 18:24–28
59. Hajiesmaili E, Clarke DR. 2019. *Nat. Commun.* 10:183
60. Mailen RW, Wagner CH, Bang RS, Zikry M, Dickey MD, Genzer J. 2019. *Smart Mater. Syst.* 28(4):045011
61. Warner M. 2019. *J. Phys. Commun.* 3:065005
62. Gu J, Breen DE, Hu J, Zhu L, Tao Y, et al. 2019. In *CHI Conference on Human Factors in Computing Systems Proceedings, Glasgow, Scotland, May 4–9*, Paper No. 37. **https://doi.org/10.1145/3290605.3300267**
63. Zeng H, Wani OM, Wasylczyk P, Kaczmarek R, Priimägi A. 2017. *Adv. Mater.* 26:1701814
64. Wani OM, Zeng H, Priimägi A. 2017. *Nat. Commun.* 8:15546
65. Lahikainen M, Zeng H, Priimägi A. 2018. *Nat. Commun.* 9:4148
66. Wani OM, Verpaalen R, Zeng H, Priimägi A, Schenning APHJ. 2019. *Adv. Mater.* 31:1805985
67. Wang X, Guest SD, Kamien RD. 2019. arXiv:1902.10835
68. Modes CD, Warner M. 2012. In *Emerging Liquid Crystal Technologies VII*, ed. L-C Chien. *Proc. SPIE Conf. Ser.* 8279:82790Q